Chapter 4

Experimental Approach

4.1 Introduction

The experimental studies described in this thesis were made using the low-speed research compressor at the University of Tasmania. In recent times, low-speed testing in similar facilities have played a large role in the design of gas turbine engines. Wisler and co-workers [189, 191] give numerous examples of how low-speed testing can provide information on a range of complex fluid flow phenomena occurring in practical turbines and compressors. Low-speed testing can also be particularly useful in validating design concepts and methodologies.

Although the flow condition in low-speed turbomachines differs from practical turbomachines which operate at high-speed and temperature, and must often satisfy size and weight constraints, many types of flow phenomena remain similar in nature. Wisler et al. [191] note that low-speed testing cannot account for phenomena that arise from compressible flow effects, including shock waves and associated interactions. However, the flow through low-pressure turbines and the intermediate and high-pressure stages in compressors is generally subsonic; here these effects are less significant.

The flow inside both low-speed and high-speed turbomachinery is highly three-dimensional. Cumpsty [24] explains how fluid viscosity affects the flow by introducing undesirable flow features often referred to as *secondary flows*. The flow through a blade passage often becomes highly three-dimensional toward the blade endwalls where suction surface boundary layers often separate in localised regions. These separations, also called *corner separations*, *vortices* or *stalls*, can lead to a spanwise variation of

flow deviation with overturning close to the endwalls. A study by Wisler et al. [190] provided some insight into the role of secondary flows in mixing processes inside a multi-stage compressor. A chemical gas tracer was introduced at several locations inside a stator blade passage and the resulting concentration was measured at downstream locations. The study concluded that both turbulent diffusion and secondary flows were responsible for mixing of the flow, and that the latter was more significant near blade endwalls.

Another common type of secondary flow near blade endwalls is caused by fluid flow through the small clearance at the tip of rotor blades. This flow generates a trailing vortex which significantly enhances downstream mixing processes. The strength and behaviour of tip leakage flow can be influenced by casing treatments, such as slots machined into casing walls. Both corner stalls and tip leakage flows make significant contributions to the overall loss in total pressure. Much research attention is currently aimed at understanding the nature of these secondary flows, their associated loss mechanisms, and ways of reducing their influence.

Many current design methods now employ three-dimensional blade design, where required, to minimise secondary flows and losses. An example of this was given by Gallimore et al. [46, 47] who used three-dimensional blading in the design of a multi-stage compressor. Detailed performance comparisons were made between this compressor design and a baseline compressor designed with conventional two-dimensional blading. The study showed that three-dimensional blade shapes could be used to improve compressor performance. The most significant improvements were made in the flow near the blade endwalls, which resulted in greater spanwise uniformity of flow. The three-dimensional CFD modelling was not very successful at predicting absolute performance, but did indicate which changes would result in beneficial flow behaviour.

The secondary flows described above add considerable complexity to the flow field. While these flows are important in terms of losses and performance, this research is concerned with the flow behaviour at mid-span height where the flow is mostly free from the effects of the endwall secondary flows. Measurements detailed by Oliver [122] in the UTAS research compressor showed that the spanwise distribution of total pressure became increasingly non-uniform at high compressor loading, particularly near the blade endwalls. This trend is consistent with other studies which show that corner stalls become larger with increasing blade loading. Oliver [122] also showed that as loading was increased to near stall, the adverse pressure gradient across the

stator blade row resulted in separation of the hub boundary layer. This effectively contracted the primary flow streamtube, resulting in a lower level of diffusion across the stator blade row. The lower diffusion also reduced the amount of separated flow on the suction surface which would normally be expected at very high incidence.

Despite this, the flow at mid-span height is well predicted by simple blade-to-blade solvers. Solomon [154] found good agreement between surface velocity distributions obtained from surface pressure tappings and a two-dimensional inviscid flow solver. This highlights the two-dimensional nature of the flow at mid-span height.

This chapter describes the rationale and approach used in the experimental investigations of this thesis. The first four sections discuss specific issues in relation to low-speed testing: inlet turbulence level, blade row clocking, compressor loading and Reynolds number. Following these sections, explanation is given on some measurement techniques and on the treatment of experimental data.

4.2 Inlet Turbulence Level

There are significant differences between the flow environment inside single-stage research compressors and commercial multi-stage compressors. It is advantageous, where possible, to make the research environment as similar as possible to the multi-stage environment. Place et al. [131] investigated how the flow in a single-stage compressor could be made more more representative of flows in multi-stage machines. Several modifications were made to the single-stage compressor: thickening the wall boundary layers by attaching rows of metal teeth to hub and casing walls, raising the inlet turbulence level by placing a turbulence grid upstream from the compressor stage, and simulating the pressure loss associated with downstream blade rows by placing a screen downstream from the compressor.

In their study, Place et al. [131] measured differences in time-mean performance and flow properties resulting from the wind tunnel modifications. However the present study is primarily concerned with flow behaviour at mid-span height. The flow at this position is most greatly influenced by turbulence level. Thus, a similar approach was taken to artificially raise the turbulence level by installing a grid at the compressor inlet. This was designed to yield similar turbulence properties to the flow in multi-stage compressors measured by Camp and Shin [18]. Details of the grid design and installation are given in Section 3.6 and Appendix B.

The influence of increased turbulence level on the unsteady flow field in the rotor–stator axial space is investigated in Chapter 5. Measurements of the flow field at high turbulence level are compared with previous measurements at low turbulence level. The influence of turbulence level on the unsteady boundary layer development on a C4 stator blade is discussed in Chapter 6. This investigation compares stator boundary layer behaviour at high turbulence with previous measurements at low turbulence. The study also examines the effect of turbulence on IGV–stator blade row clocking. The turbulence grid was also used in testing with the CD stator blade row as detailed in Chapter 7.

4.3 Blade Row Clocking

In multi-stage turbomachinery it is possible to have adjacent rows of rotor or stator blades with equal numbers of blades. This type of configuration leads to a pitchwise periodic variation of flow properties. Some researchers have suggested that performance may be improved with appropriate circumferential alignment or *clocking* of these blade rows.

The UTAS research compressor is well suited for studies of blade row clocking effects. As explained in Chapter 3, both the IGV and stator blade rows are held in movable rings that allow circumferential traversing relative to a fixed probe position. These blade rows also have an equal number of blades, which causes all blade row elements to experience the same pitchwise flow field for a given alignment of the IGV and stator blade rows. This pitchwise periodicity was also maintained in testing with the CD stator blade row, since the CD stator blade row contained exactly half the number of blades in the C4 stator blade row. Individual IGV and stator blade elements will experience different rotor passing phases due to the differing number of rotor blades.

Figure 4.1 shows a cross-section of the research compressor with the C4 stator configuration. A typical wake dispersion pattern based on flow observations by Lockhart [106] has been overlaid to show the various blade row clocking scenarios. The variable (g) indicates the distance between grid wake centreline and the IGV blade stagnation streamline. The case $g/S = 0.5$ corresponds to the grid wakes centred in the IGV passage and the case $g/S = 0.0$ corresponds to the grid wakes incident on the IGV blade row. Similarly, the variable (a) indicates the distance between IGV

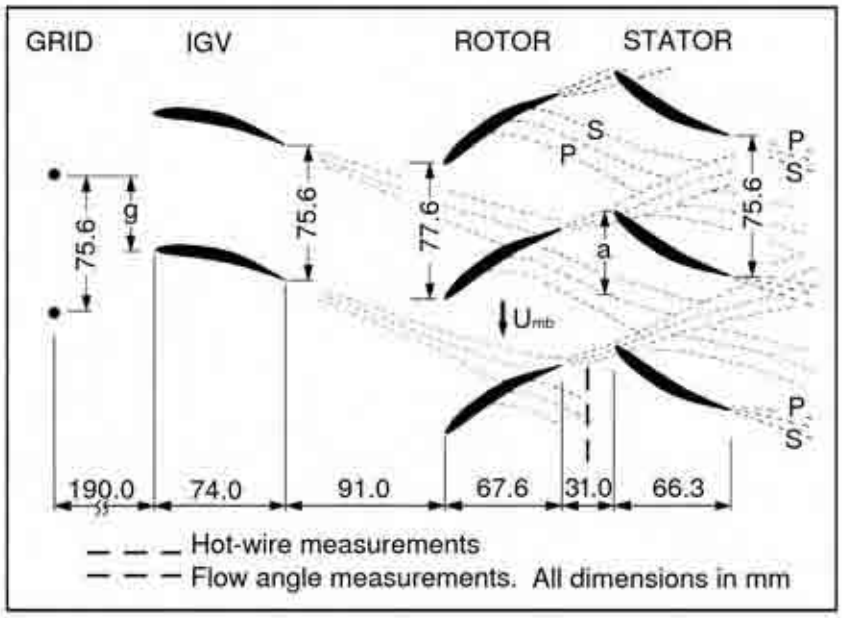

Figure 4.1: Cross-section of the research compressor showing mid-span blade row configuration and typical instantaneous wake dispersion pattern (C4 stator)

blade wake centrelines and the stator blade stagnation streamline. Likewise, the case $a/S = 0.5$ corresponds to the IGV wakes centred in the stator passage and $a/S = 0.0$ corresponds to the IGV wakes incident on the stator blade row. These clocking cases were used in the experimental investigations detailed in Chapters 5 and 6.

4.4 Compressor Loading

Gas turbine engines must have satisfactory performance over a wide range of operating conditions. Cumpsty [24] discusses the difficulty posed in achieving high efficiency at design conditions while maintaining satisfactory performance under off-design conditions. The performance of an individual blade row is a strong function of flow incidence and thus loading.

Three compressor loadings were chosen for detailed studies of the aerodynamic flow over the C4 stator blade row: high ($\phi = 0.600$), medium ($\phi = 0.675$) and low ($\phi = 0.840$). These loadings were representative of near stall, design, and maximum flow, respectively. The same test cases were used in previous investigations by Walker and co-workers [85, 158, 180, 181]. Use of these test cases in the present study allowed

direct comparisons to be made with measurements from previous investigations. The influence of loading on stator inlet flow field is detailed in Chapter 5. The effect of blade loading on the aerodynamic behaviour of both C4 and CD stator blades is described in Chapters 6 and 7, respectively. A slightly different set of test load cases was chosen for testing with the CD stator blade row. The rationale for this is explained in Chapter 7.

4.5 Reynolds Number

The aerodynamic performance of a blade row is strongly influenced by Reynolds number. Low-speed turbines and compressors used for research often operate at significantly lower Reynolds numbers than practical turbomachines. Figure 4.2 shows a typical variation of Reynolds number in a turbofan engine at altitude cruise. The blade chord Reynolds number in the compressor section ranges typically from $0.6(10)^6 - 1.2(10)^6$. By comparison, the majority of testing in the UTAS research compressor were performed at considerably lower Reynolds numbers ($Re_1 \approx 1.2(10)^5$ for the testing with the C4 stator and $Re_1 \approx 3.0(10)^5$ for testing with the CD stator). The use of lower Reynolds numbers in research compressors is common, but not without criticism. The implications of testing at lower Reynolds numbers must be carefully studied so that the effect on resulting flow behaviour is well understood.

One method of increasing the Reynolds number in low-speed research turbomachinery is to increase the size of model geometry. In general, the blading in research turbines and compressors is usually several times larger than in practical turbomachines. This also has the benefit of allowing measurement of small scale fluid flow phenomena, such as blade boundary layers, with instruments of practical size. This approach was used in the design of the CD stator which had a chord length of twice the C4 stator.

Cumpsty [24] summarises an experimental investigation by Rhoden [134] in which the flow behaviour of a C4 aerofoil cascade was studied at near design operation over a range of Reynolds numbers. In general, the flow over the suction surface was more greatly influenced by Reynolds number. At a Reynolds number of $1.8(10)^5$, the flow remained laminar past mid-chord position where a large perturbation in the pressure coefficient clearly indicated the presence of a separation bubble. As the Reynolds number was reduced to $0.6(10)^5$, transition moved upstream and the

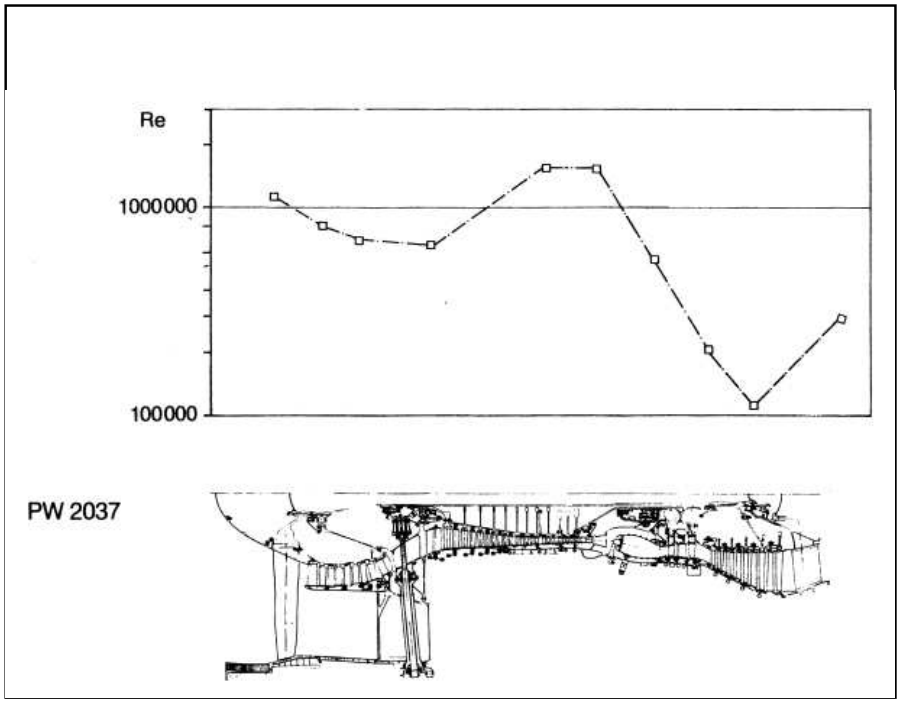

Figure 4.2: Reynolds number variation in the PW2037 high bypass ratio turbofan at altitude cruise (from Hourmouziadis [79])

separation bubble grew in size. Further reducing the Reynolds number caused the separation bubble to increase until the boundary layer no longer reattached. This resulted in a massive loss of performance, which was apparent at a Reynolds number of $0.3(10)^5$. This is commonly referred to as the *critical Reynolds number* and would likely have occurred for a Reynolds number in the range $0.3(10)^5 - 0.6(10)^5$. At a higher Reynolds number of $4.8(10)^5$, the separation bubble became smaller and overall losses were decreased. The study also showed that the benefit of decreasing loss with increasing Reynolds number became less at high Reynolds number. The losses were only marginally reduced beyond a Reynolds number of $2.0(10)^5$.

The effect of Reynolds number on the stator blade behaviour in the UTAS research compressor was studied by Solomon [154]. Hot-film and surface pressure measurements of C4 stator blades were made at three different reference Reynolds numbers (Re_c): low ($0.6(10)^5$), medium ($1.2(10)^5$) and high ($1.7(10^5)$). The hot-film measurements were processed to yield the temporal variation of ensemble average intermittency. The intermittency distributions at medium and high Reynolds numbers were very similar on the suction surface. A slightly greater level of turbulent flow was observed on the pressure surface in the high Reynolds number case. The intermittency distribution at

low Reynolds number differed significantly from the other cases, and the intermittency detection algorithm had difficultly in distinguishing between laminar and turbulent signals. The measured surface pressure distribution also showed close similarity between medium and high Reynolds number cases. The study concluded that the flow in the medium Reynolds number case was super-critical. This is also consistent with the C4 cascade studies by Rhoden [134]. Additional studies of flow behaviour at this Reynolds number are reported by Hughes [83] and in Chapters 5 and 6 of this thesis.

The studies by Rhoden [134] and Solomon [154] highlight the influence of Reynolds number on flow behaviour. As noted by Solomon [154], the critical Reynolds number will depend largely on blade design. At normal operating conditions, C4 section blades have a suction peak very close to the leading edge which is followed by a approximately linear deceleration over most of the suction surface. Designs of this nature would be expected have lower critical Reynolds numbers than designs based on modern controlled diffusion approach, where peak suction occurs further downstream and diffusion takes place over a much shorter distance. Halstead et al. [61] recommend that low speed testing should be carried out for stage-average Reynolds numbers greater than $3(10)^5$. With this in mind, testing with the CD stator in Chapter 7 was performed over a suitable range of Reynolds numbers to ensure that Reynolds number effects were understood and that all relevant testing was performed above the critical Reynolds number.

4.6 Total Pressure and Flow Angle

Measurement of total pressure and flow angle in axial turbomachinery can provide useful information about losses and performance. In this study, measurements of time-averaged total pressure and flow angle were made at mid-span in the rotor–stator axial space. The total pressure measurements allowed stator surface velocities to be determined from measured surface pressure distributions. The flow angle measurements were used in boundary conditions for various computational studies.

The total pressure and flow angle were measured using a commercial three-hole cobra probe. Details of this instrument and calibration are provided in Section 3.4.8. Solomon [154] also used this instrument to measure the total pressure in the rotor–stator axial space. The total pressure measurements were repeated using a Kiel probe which is known to be relatively insensitive to flow direction. Solomon [154] found only

minor differences between measurements from both instruments and concluded that the three-hole probe could be used to measure total pressure with sufficient accuracy. Figure 4.3 shows the variation of total pressure with clocking position at various compressor loadings as measured by Hughes [83].

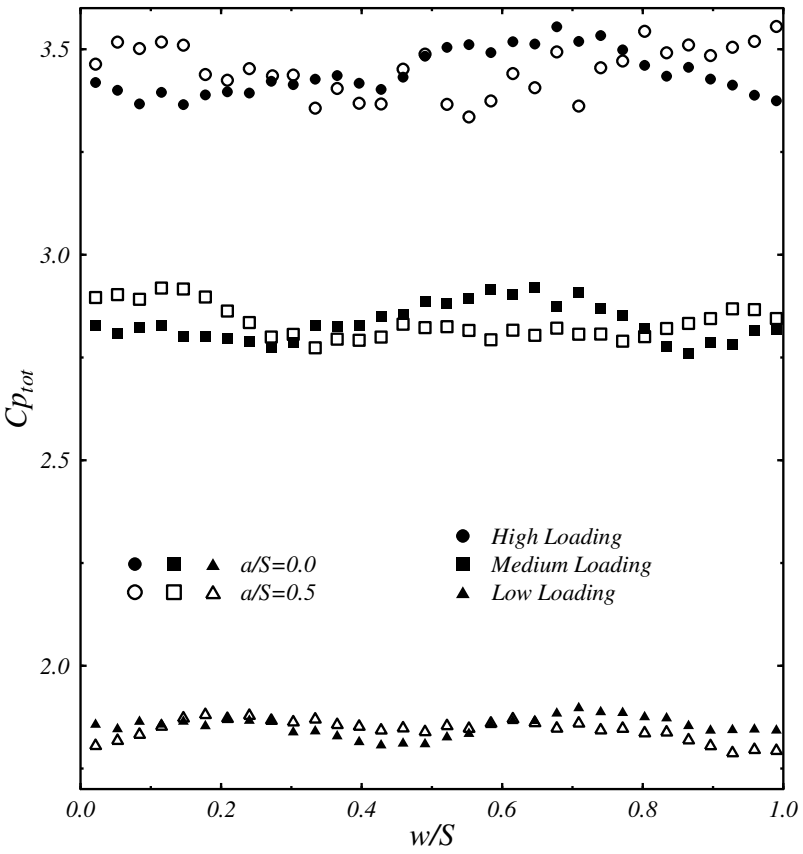

Figure 4.3: Pitchwise variation of total pressure coefficient in the rotor–stator axial gap at mid-span. Three-hole probe measurements 20.7%c axially upstream from the stator leading edge (from Hughes [83], $Re_c = 120000$)

The total pressure distribution in the rotor–stator space had been previously measured by moving both IGV and stator blade rows together in equal steps over a blade passage relative to a circumferentially fixed probe. The effect of IGV–stator clocking on the total pressure was measured by simply changing the relative alignment between the blade rows. However, the addition of the turbulence grid, having the same number of elements as the IGV blade row, generated a new clocking scenario resulting from the relative alignment between the turbulence grid and IGV blade row. It followed that application of the existing procedure would result in additional clocking effects between grid and IGV blade row.

In order to quantify the strength of the grid–IGV clocking effect, pitchwise distributions of total pressure were measured in the rotor–stator axial space for various fixed alignments of the grid and IGV. These measurements could not be performed using a probe that was circumferentially fixed since the design of the research compressor did not permit circumferential traversing with an externally inserted probe. Instead, the total pressure was measured using a thin walled stainless steel tube, attached to a CD stator blade at mid-span height and aligned in the centre of the rotor–stator axial space. The tube was aligned to the flow direction with an estimated accuracy of $\pm 5^\circ$. The survey was completed by clocking the probe and stator over a single blade passage. The wind tunnel experiments by Gracey [57] showed that a thin walled tube aligned within $\pm 11^\circ$ of the flow direction can measure total pressure with an error less than $\pm 1\%$ of dynamic pressure.

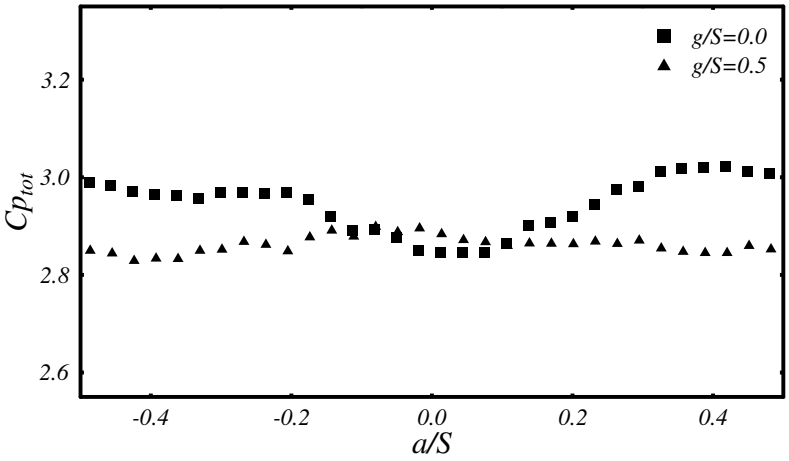

Figure 4.4: Pitchwise variation of total pressure coefficient with grid–IGV alignment in the rotor–stator axial gap at mid-span height. Total pressure tube measurements at 18.7%c axially upstream from the CD stator leading edge (based on C4 chord length, $Re_c = 120000$, $\phi = 0.675$)

Figure 4.4 shows the measured total pressure coefficient for two different alignments of the grid and IGV blade row. The case $g/S = 0.0$ corresponds to aligning the grid wakes on the IGV blade row and the case $g/S = 0.5$ corresponds to aligning the grid wakes in the IGV passage. A significant variation in total pressure is observed in the $g/S = 0.0$ clocking case with minimum total pressure occurring at $a/S = 0.0$. This is not surprising since the total pressure loss associated with the grid wakes is aligned with the IGV wake street, resulting in a large deficit of total pressure at $a/S = 0.0$. In contrast $g/S = 0.5$ results in a much more uniform distribution of total pressure.

The measurements presented in Chapter 5 show this configuration results in a more uniform velocity and turbulence field.

After considering these results, all surveys of total pressure and flow angle were performed using a new method. Since the experimental apparatus did not allow traversing of probes in the pitchwise direction, the measurements were made by leaving the IGV fixed at $g/S = 0.5$ and indexing the stator blade row in 32 equal steps over one blade pitch. The measurements of total pressure coefficient and flow angle were averaged to remove effects associated with the potential field of the stator blade row. It is recognised this does not provide a direct measurement of the pitchwise flow field; however, it has the advantage of avoiding significant clocking effects that arise from moving the IGV blade row relative to turbulence grid. The pitchwise averaged total pressure coefficient obtained from this method was found to agree within 1.5% of the pitchwise averaged total pressure coefficient measured using the simple total pressure tube. The total pressure coefficient at a given circumferential position in the rotor–stator axial space was observed to vary by no more than 2% of the pitchwise average total pressure coefficient.

4.7 Blade Surface Pressure Measurements

Surface pressure tappings provide useful information about the time-average flow around the blade surface. In this thesis, surface pressure distributions were measured at mid-span on a CD stator blade and also on the suction surface of a C4 stator blade. All surface pressure tappings and reference pressures were connected to a Scanivalve pneumatic switching valve. Response times for individual ports were measured by switching across a known pressure differential and recording the response time. In general, a 99% response was achieved within a 30 second settling time. An average pressure at each station was obtained by averaging 300 readings sampled at 5 Hz. This relatively long sampling period was deemed necessary considering the long-term variation of flow coefficient described in Section 3.5.2.

A local static pressure coefficient for each blade surface pressure (p_i) may be expressed as

$$Cp_i = \frac{p_i - p_{in}}{P_{in} - p_{in}} = \frac{p_i - p_{in}}{\frac{1}{2}\rho V_a^2} \tag{4.1}$$

where the subscript *in* indicates the conditions at compressor inlet. The surface velocity may be determined from

$$\frac{U}{U_{mb}} = \phi\sqrt{Cp_{tot} - Cp_i} \tag{4.2}$$

where Cp_{tot} is the total pressure coefficient and $\phi = V_a/U_{mb}$ is the compressor flow coefficient defined in Section 4.6. The rotor blade speed (U_{mb}) is used for normalising surface velocity to allow direct comparison with the previous results of Solomon [154] and Hughes [83].

4.8 Stator Inlet Reynolds Number

The stator inlet Reynolds number (Re_1) in the research compressor is an important parameter influencing the viscous flow behaviour of the stator blade row. It is also required to convert predicted blade surface distributions to the form given in Eq. (4.2) for comparison with experimental measurements.

Solomon and co-workers [154, 158] determined the stator inlet Reynolds number using the following approximate correlation

$$Re_1 = Re_c\left(\frac{\phi}{\cos(\alpha_1)}\right) \tag{4.3}$$

where the stator inlet flow angle α_1 was determined by mass-averaging axial and peripheral velocity components measured by three-hole probe surveys across the passage.

Despite the approximate nature of Eq. (4.3), it was found to give good agreement in comparing measured and predicted stator surface velocity distributions for both the C4 and CD stators.

4.9 Presentation of Hot-Wire Measurements

In this study, hot-wire measurements were processed using a statistical technique based on ensemble or phase-lock averaging. This technique was developed by Evans [42] and has since been used in numerous studies by Walker and co-workers [67, 180, 181]. A brief summary of the method follows.

Instantaneous velocity is often expressed in terms of a time-mean $\overline{u}$ and associated

fluctuating component u'.

$$u = \overline{u} + u' \tag{4.4}$$

Since the flow inside turbomachines is characterised by strong periodic events, the instantaneous velocity may alternatively be defined in terms of an ensemble-averaged velocity $\langle u \rangle$ and associated fluctuating component u''. This may be expressed as

$$u = \langle u \rangle + u'' \tag{4.5}$$

The ensemble-averaged velocity obtained from N observations at phase t_i relative to the start of sampling is given by

$$\langle u \rangle(t_i) = \frac{1}{N} \sum_{k=1}^{N} \{u(t_i)\}_k \tag{4.6}$$

The ensemble-averaged velocity field is pitchwise periodic owing to equal blade elements in the IGV and rotor blade rows. This periodicity in the pitchwise direction has a wavelength equal to the IGV–stator blade pitch. The periodic disturbance level or 'unsteadiness' of the ensemble mean about the time-mean must be evaluated over an integral number of blade passing periods. This may be non-dimensionalised by the local free-stream velocity U and is expressed by

$$\tilde{T}u = (\langle u \rangle - \overline{u})_{RMS}/U \tag{4.7}$$

The random unsteadiness or turbulence level is given by

$$Tu = \left(u''\right)_{RMS}/U \tag{4.8}$$

The total disturbance level or 'apparent' turbulence is given by

$$Tu_D = \left(u'\right)_{RMS}/U \tag{4.9}$$

Assuming that the periodic and random components of turbulence are statistically independent they may be related by

$$Tu_D^2 = \tilde{T}u^2 + Tu^2 \tag{4.10}$$

4.10 Presentation of Hot-Film Measurements

Interpretation of flow behaviour from surface mounted hot-film sensor measurements is a very challenging task. In most cases it is not practical to individually calibrate sensors once they are rigidly attached to a complex surface such as a turbomachinery blade. An alternative approach developed by Hodson et al. [76] uses a quasi wall shear stress (τ_q) obtained from uncalibrated hot-film sensors that is proportional to the actual wall shear stress (τ_w). The quasi wall shear stress is simply derived from the raw anemometer bridge voltage E by

$$\tau_q = \left(\frac{E^2 - E_o^2}{E_o^2} \right)^3 \propto \tau_w \tag{4.11}$$

where E_o is the anemometer bridge voltage corresponding to zero flow. Many experimental studies have used this approach, including Halstead et al. [61, 62].

Measurements of quasi wall shear stress from uncalibrated sensors may be interpreted to indicate laminar–turbulent flow behaviour. Many methods have been developed to achieve this objective. Solomon and Walker [155] used several different methods to process data from hot-film sensors on a compressor stator blade. These included the flatness factor or 'kurtosis', a modified form of the TERA method developed by Falco and Gendrich [43], and also various forms of normalised quasi wall shear stress. Of these methods, the TERA method for determining turbulent intermittency was found to give the clearest differentiation of laminar and turbulent flow but had the disadvantage of needing manual adjustment of the detector function threshold for each sensor.

Solomon and Walker [156] later proposed a new method of determining turbulent intermittency without any need for manual adjustment of sensor thresholds. This method used a hybrid approach that combined the probability density function (PDF) method of Hazarika and Hirsch [65] with the peak-valley counting (PVC) method of Zohar and Ho [201]. This PDF/PVC method was used for analysis of hot-film measurements in the present study, and is summarised in the following paragraphs.

The first step is to classify the quasi wall shear stress trace into laminar or turbulent parts depending on the characteristics of the signal. A detector function is defined as the derivative of the quasi wall shear stress with respect to time ($D = \delta\tau_q/\delta t$). The intermittency distribution is set to zero and an initial threshold for the detector function is set to $0.7(D)_{RMS}$. Parts of the trace where the detector function exceeds this

threshold are examined for occurrences of peaks and valleys which are characteristic of high frequency turbulent fluctuations. Regions where peaks and valleys occur within a predefined window period are assigned an intermittency value of 1. This provides an initial estimate of the intermittency distribution.

Selection of the window period must take into account the sampling frequency used in data acquisition and also the characteristic frequency of the turbulent fluctuations. A detailed discussion of window period selection is given by Solomon [154].

Once an initial estimate of the intermittency distribution is known, an iterative process is used to optimise the detector function threshold. The first stage is to calculate the probability density functions (PDF) for the respective laminar and turbulent parts. These are assumed to be Gaussian distributions. A new threshold is defined at the intersection of the laminar and turbulent Gaussian distributions. This updated value is used to re-evaluate the intermittency distribution. The process is repeated until the threshold has converged to an acceptable level of accuracy. A relaxation factor is used to update the threshold. This aids in damping oscillations in the solution process.

The calmed flow following the passage of a turbulent spot is characterised by a higher shear stress than laminar flows [150]. As the calming effect wears off, the shear stress reduces asymptotically to a laminar level. Solomon [154] realised this behaviour could also be identified in surface hot-film measurements. In addition to the laminar–turbulent identification, relaxing flow is assumed to occur following positive identification of turbulent flow while the shear stress is continuously decreasing. Detection of relaxing flow is terminated by the first increase in τ_q.

The variability in the strength and timing of individual rotor wake disturbances leads to significant variation of the wake-induced transition process occurring on a blade surface. A more reliable indication of periodic events is provided by ensemble or phase-lock averaging a large number of individual records, each acquired at a particular rotor phase on separate rotor revolutions. This method was used in this thesis to obtain temporal variations of ensemble average intermittency and relaxing flow. In summary, the intermittency detection algorithm developed by Solomon [154] provides a reliable method for determining transitional flow behaviour with minimal manual intervention.

4.11 Blade Surface Particle Trajectories

It is common to show time-varying quantities around a blade surface in the form of a time $\sim$ distance plot. This approach is used in this thesis to show temporal variations of ensemble averaged intermittency around the surface of a stator blade. In these plots it is also useful to show the time $\sim$ distance trajectory of particles travelling at various fractions of free-stream velocity. These can then be used to interpret the leading and trailing edge celerities of turbulent strips.

The time taken for a particle to travel along a blade surface between surface length positions s_1^* and s_2^* may be determined by integration of the surface velocity distribution. This may be expressed in terms of a non-dimensional velocity by

$$t^* = C \int_{s_1^*}^{s_2^*} \frac{1}{U^*} ds^* \tag{4.12}$$

where the dimensionless velocity is defined as $U^* = U/U_{mb}$ and the dimensionless constant is given by $C = s_{max}/(T\ U_{mb}) = (37\ s_{max})/(2\ \pi\ R_{mb})$

Inspection of Eq. (4.12) shows that the integrand will be undefined near the leading edge where the flow stagnates ($U^* = 0$). This was overcome in this investigation by beginning the calculation a short distance downstream from the leading edge ($s^* = \pm 0.02$) and aligning the trajectory with the centre of the observed wake trajectory. This approach was also used by Solomon [154].

Chapter 5

Stator Inlet Flow

5.1 Introduction

It is widely recognised that unsteady flow effects influence vibration, noise generation and the aerodynamic performance of axial turbomachinery. Unsteady flow arises due to the relative motion between adjacent blade rows. Doorly and Oldfield [32] describe three main sources of unsteady flow. The first is caused by the relative movement of pressure fields generated by adjacent moving and fixed blade row elements. The influence of these fields can extend both upstream and downstream from a blade row, inducing fluctuations in both flow velocity and pressure. The magnitude of this phenomenon depends largely on the blade loading and the axial spacing between rows. The second source is common in the first stage of turbines and compressors where the flow often reaches transonic speed, leading to the formation of compressible shock waves. Shock waves can interact with other blades in the same blade row or appear as travelling waves to neighbouring blade rows. The third source of unsteadiness, the main focus of the present investigation, is caused by the dispersion of viscous wakes shed from upstream blade rows. These wakes convect with the free-stream flow and are chopped and rotated as they pass through downstream blade row passages. Smith [153] observed this process in a four-stage research compressor, describing it as 'wake dispersion'. Adjusting the relative alignment between neighbouring stationary blade rows was found to significantly alter the downstream flow field.

Several studies of unsteady flow have been made using the UTAS low-speed research compressor. Lockhart and Walker [107] used a hot-wire probe to measure the unsteady flow field in the rotor–stator axial space. This investigation showed the

thickness of rotor wakes varied periodically with streamwise position. Lockhart and Walker [107] suggested this was due to an interaction between IGV and rotor wakes and proposed a physical model describing the observed 'wake–wake' interaction. More detailed investigations were later carried out by Walker et al. [180, 181] with the aid of high-speed data acquisition and digital processing. These studies showed that an interaction between IGV and rotor wakes developed downstream from the rotor trailing edge and resulted in a local accumulation of highly turbulent rotor wake fluid toward the suction side of the IGV wake street.

As rotor wakes convect through the a downstream stator blade row, the relative convection of fluid within the wakes (negative jet) is interrupted by the stator blade row. Kerrebrock and Mikolajczak [94] studied this effect in a low-speed research compressor. A small amount of helium gas was released from small holes close to the trailing edge of two rotor blades. Time-mean concentrations of helium gas were measured downstream from the stator blade row. A higher concentration of helium was measured on the pressure side and a lower concentration was measured on the suction side. This qualitatively agreed with their model which predicted an accumulation of wake fluid on the pressure side, and a corresponding decrease on the suction surface. The flow measurements by Walker et al. [180, 181] indicated only a small accumulation of rotor wake fluid close to the stator trailing edge. The fact the accumulation occurred over a streamwise distance suggests the effect is primarily caused by an interaction between rotor and stator blade wakes.

Wake–wake interaction was also studied in a two-stage axial pump by Chow et al. [21]. Particle image velocimetry (PIV) measurements showed a strong interaction between IGV and rotor wakes resulted in turbulent 'hot-spots' within the rotor wake. The wake–wake interaction was much stronger than observed by Walker and coworkers. However, this may be partially explained by the differing compressor designs in the test facilities.

Numerous studies have focused on the unsteady flow through turbine blade rows. Doorly and Oldfield [31, 32] studied the effects of shock waves and wakes shed by an upstream nozzle guide vane (NGV) through a downstream rotor blade row in a transient cascade tunnel. The NGV wakes were simulated by wakes generated from a row of moving bars attached to a rotating disk. Measurements using Schlieren photography, unsteady pressure measurements and rotor surface heat transfer measurements were interpreted to provide time-resolved information about the flow field. The study

showed the rotor wakes underwent 'massive' distortion as they passed through the rotor blade passage. Both shock waves and convective wake disturbances were found to initiate turbulent patches in a rotor blade boundary layer: these were observed at different instants since shock waves travel at sonic speed and wake disturbances convect with the local free-stream.

A more recent study by Stieger and Hodson [163] used laser Doppler anemometry (LDA) to investigate the passage of a wake through a low-pressure turbine cascade. Upstream wakes were generated by a row of bars attached to a moving belt. Phase-lock averaged diagrams of turbulence kinetic energy and velocity vector fields were shown at several instants during a wake passing period. These results provided detail of how the wake was bowed, elongated and stretched as it passed through the blade passage. The high level of distortion caused wake fluid to spread across a large portion of the blade suction surface. This was further investigated by Opoka and Hodson [125] who increased the background turbulence level inside the cascade to approximately 4% by placing a turbulence grid at the wind tunnel inlet. The increased turbulence level was found to decrease the maximum level of turbulent kinetic energy present in the wakes. These studies highlight significant differences between wake dispersion processes occurring in turbines and compressors.

This chapter investigates the unsteady flow field at entry to the stator blade row of the UTAS research compressor. Particular focus is given to the influence of turbulence on wake dispersion and wake–wake interaction processes. The level of background turbulence was raised to levels typical of an embedded stage in a multi-stage turbomachine by installing a grid at compressor inlet. The unsteady flow field in the rotor–stator axial space was measured using a single element hot-wire probe. The processed results were compared with previous measurements by Hughes [83] using the natural low turbulence inflow configuration. Significant conclusions are drawn about the influence of free-stream turbulence on wake dispersion and interaction processes.

5.2 Experimental Technique

The stator inlet flow field was surveyed using a single element Dantec 55P05 hot-wire probe aligned in the radial direction and axially positioned in the centre of the rotor–stator space. Details of the probe calibration method are given in Section 3.4.6.

Measurements were made at three compressor load cases: low ($\phi = 0.840$), medium

($\phi = 0.675$) and high ($\phi = 0.600$). The compressor was operated at a constant reference Reynolds number $Re_c = 120000$ during each test. The flow coefficient was adjusted to the required set-point before commencing each survey. The same Reynolds number and test load cases were used in previous studies by Hughes [83]: this enabled direct comparison of results.

Although the compressor operating conditions were matched in both low and high turbulence configurations, different methods were employed to survey the flow field. The surveys made using the low turbulence configuration by Hughes [83] were achieved by moving the IGV blade row in 32 steps of equal size over one blade pitch relative to a circumferentially fixed probe. The surveys using the high turbulence configuration had to be performed in a different way to avoid a clocking effect between the IGV blade row and turbulence grid. This clocking effect was confirmed by measurement of the IGV surface pressure distribution performed at various circumferential alignments of the grid and IGV blade row. These results (not presented) indicated the presence of a large separation bubble on the suction surface for a narrow range of IGV positions (typically 10% of blade pitch). This suggests the grid wakes had not fully merged at the IGV blade row resulting in a small zone of low turbulence flow. Outside this zone, IGV blade row experiences higher turbulence which may either reduce the size of the separation bubble or initiate transition before separation can occur. The clocking effect may significantly alter the flow deviation from the IGV blade row and most likely rotor and stator incidences.

In order to avoid this additional clocking effect, surveys of the unsteady flow field in the rotor–stator axial space were made by moving the probe relative to the fixed position of the IGV blade row. This was accomplished by supporting the probe in a jig that spanned between two adjacent stator blades. The hot-wire element was axially positioned in the centre of the rotor–stator axial space (20%c axially upstream from the stator leading edge) and aligned in the passage between stator blades. Both the probe and stator blade row were indexed over one blade pitch in 32 steps of equal size. A schematic diagram of this testing arrangement is shown in Fig. 5.1.

The measurements presented in Section 5.3 correspond to the clocking scenario with the grid wakes aligned in the centre of the IGV passage ($g/S = 0.5$). It is later shown in Section 5.3.1 that this achieves a more uniform turbulence distribution in the rotor–stator axial space than the case with the grid wakes incident on the IGV blade row ($g/S = 0.0$).

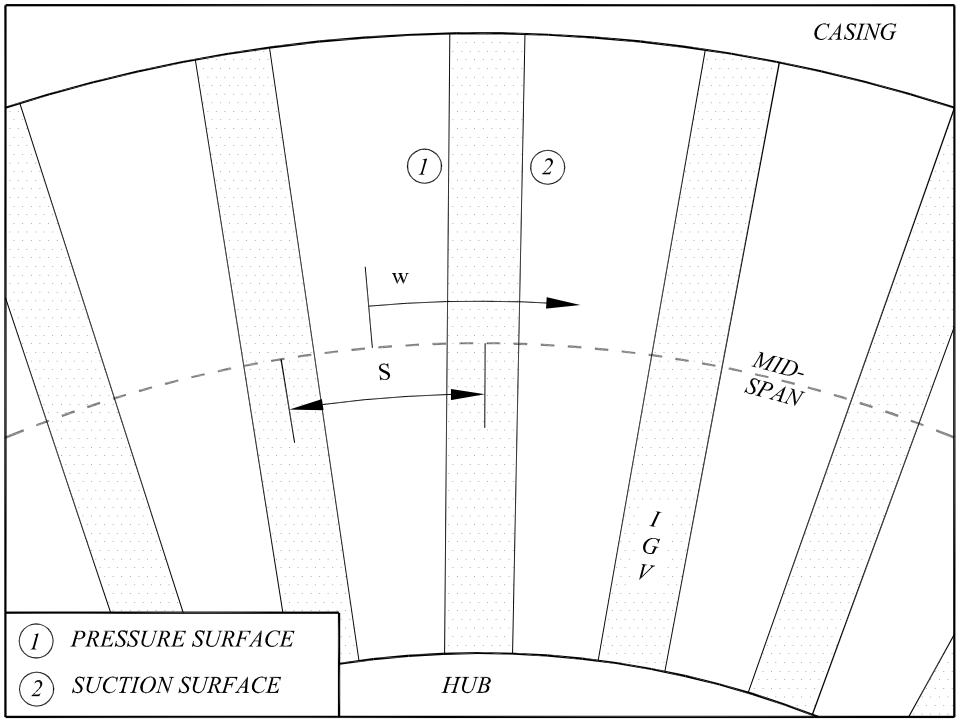

Figure 5.1: View looking upstream showing the path of the probe relative to the IGV blade row

The hot-wire probe was controlled using a constant temperature TSI–IFA100 anemometer. The offset and gain settings were optimised to maximise the voltage range for input to the data acquisition system. The frequency response of the system was measured using a square wave test to be greater than 70 kHz. All signals were low pass filtered at 20 kHz to avoid aliasing during digitisation of the data. The data acquisition process was triggered at a fixed rotor phase using a timing pulse issued from the shaft encoder. At each pitchwise position, 512 records were acquired, each on separate revolutions of the rotor. Each record contained 1024 points acquired at a sampling frequency of 50 kHz. Further detail on the data acquisition system is provided in Chapter 3.

The hot-wire probe was calibrated inside the research compressor using the in-situ method described in Section 3.4.6.

5.3 Unsteady Flow Field

The hot-wire probe measurements were processed to yield temporal variations in ensemble averaged turbulence and velocity using the method outlined in Section 4.9. The unsteady flow field for each loading case is shown in Figs 5.2–5.4. Each figure

shows the low turbulence case (upper part) and the high turbulence case (lower part). The filled colour contours show ensemble averaged velocity and the line contours show ensemble averaged turbulence level. The vertical axis indicates pitchwise position in the research compressor. The horizontal axis indicates time normalised by rotor passing period. The plots may be interpreted as an instantaneous view of the unsteady flow field on a cylindrical surface at mid-span radius resulting from the flow being convected unaltered from the measuring station with zero whirl. The line charts on the right-hand side of each plot show the pitchwise variation of time mean velocity and turbulence properties defined in Section 4.9.

The rotor wakes appear as diagonal bands with high turbulence and low velocity. The IGV wake segments are identified between the rotor wakes by higher background turbulence and are slightly rotated from horizontal. The wake dispersion pattern contrasts from that shown in Fig. 4.1 as the whirl velocity has been omitted.

The influence of compressor loading on the unsteady flow field is clearly shown in Figs 5.2–5.4. Increased compressor loading causes the rotor blade row to experience a greater flow incidence. This is reflected by the increased thickness of rotor wakes shown in Fig. 5.4. Increased loading also results in a greater amount of turning of the flow through the rotor blade row and the increased circulation causes a greater rotation of the IGV wake segments. These effects are most clearly observed in the low turbulence measurements where there is a greater distinction between turbulence in the wakes and free-stream flow.

The rotor wakes in the low turbulence measurements are observed to have temporal fluctuations in thickness and turbulence properties. Local accumulations of highly turbulent low energy fluid appear toward the suction side of the IGV wake streets. On first inspection, this may appear to be due to unsteady fluctuations in rotor blade circulation caused by an interaction between the IGV wakes and the rotor blade row. Whilst this would explain the measured fluctuations in rotor wake thickness, a more detailed explanation was provided by Hughes [83]. Surveys of the unsteady flow field in the rotor–stator axial space at several different axial positions showed little accumulation of highly turbulent rotor wake fluid close to the rotor trailing edge. Instead, the accumulation developed over a downstream distance which suggests it is caused by the relative convection of fluid in the wake jets.

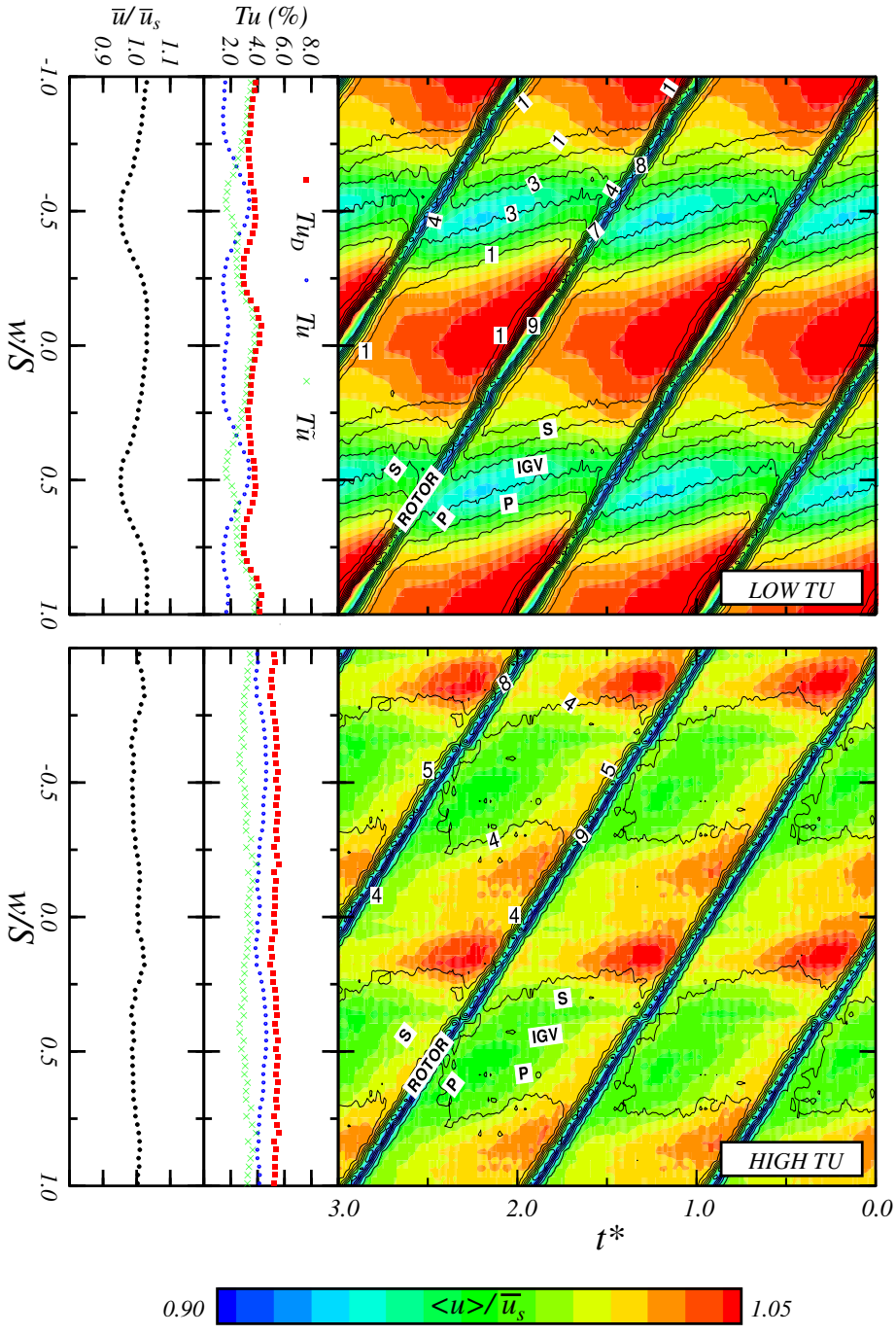

Figure 5.2: Unsteady flow field in the rotor–stator axial space at low compressor load ($\phi = 0.840$, and $Re_c = 120000$). Top: low turbulence case without grid. Bottom: high turbulence case with grid (grid wakes in IGV passage $g/S = 0.5$). Filled contours show ensemble-averaged velocity $\langle u \rangle / \overline{u}_s$. Line contours show ensemble-averaged turbulence level $\langle Tu \rangle$ in 1% intervals.

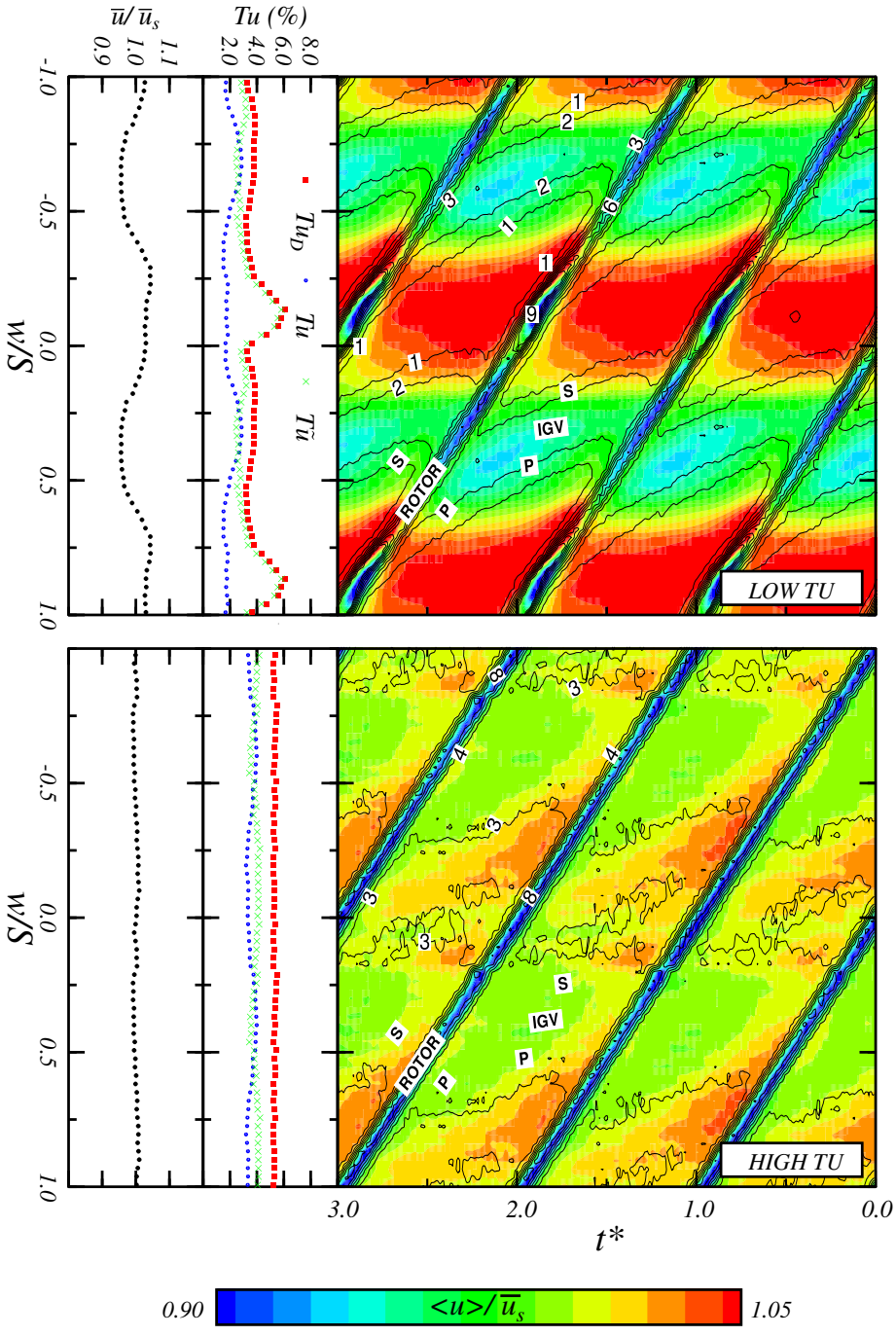

Figure 5.3: Unsteady flow field in the rotor–stator axial space at medium compressor load ($\phi = 0.675$, and $Re_c = 120000$). Top: low turbulence case without grid. Bottom: high turbulence case with grid (grid wakes in IGV passage $g/S = 0.5$). Filled contours show ensemble-averaged velocity $\langle u \rangle / \overline{u}_s$. Line contours show ensemble-averaged turbulence level $\langle Tu \rangle >$ in 1% intervals.

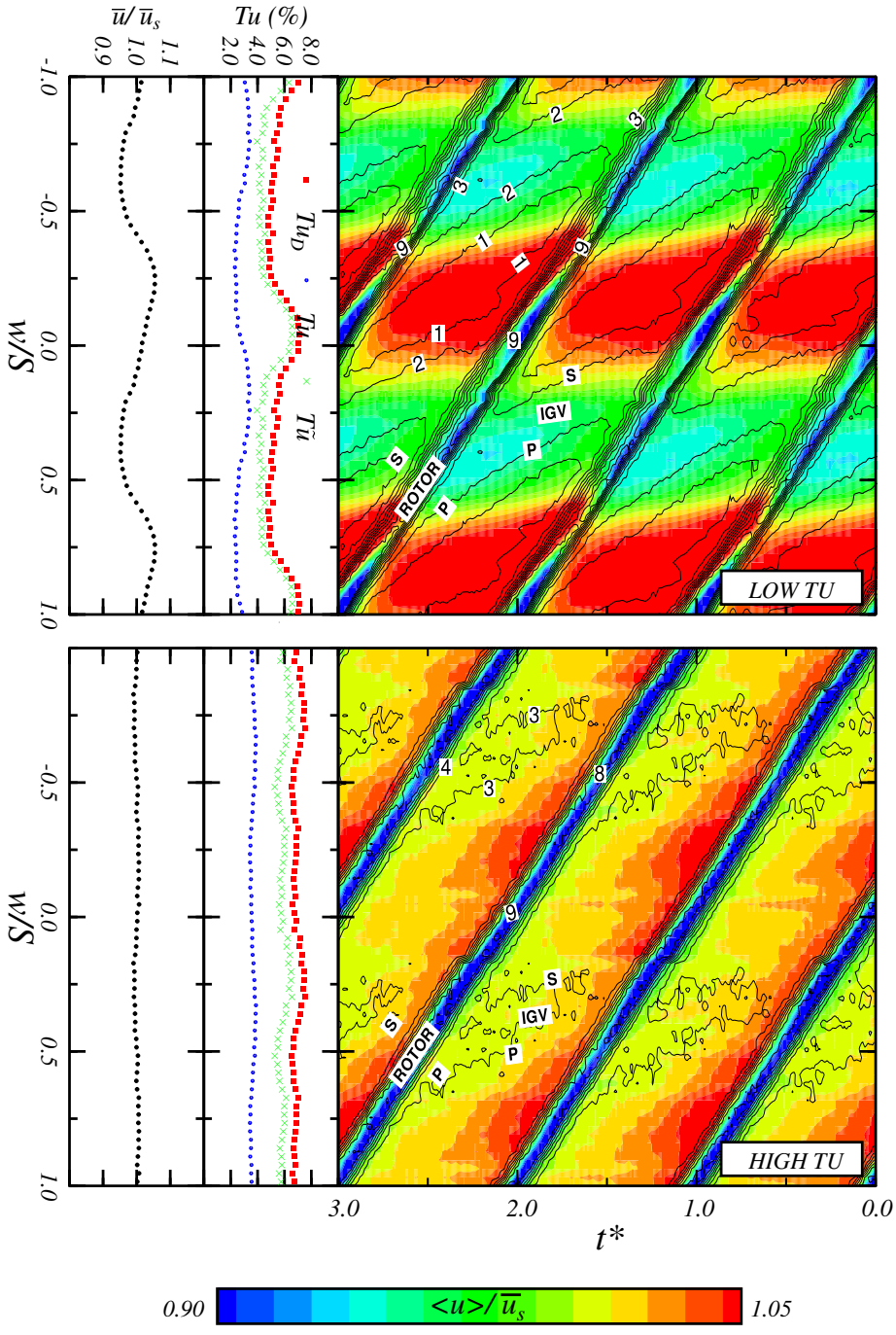

Figure 5.4: Unsteady flow field in the rotor-stator axial space at high compressor load ($\phi = 0.600$ and $Re_c = 120000$). Top: low turbulence case without grid. Bottom: high turbulence case with grid (grid wakes in IGV passage $g/S = 0.5$). Filled contours show ensemble-averaged velocity $\langle u \rangle / \overline{u}_s$. Line contours show ensemble-averaged turbulence level $\langle Tu \rangle >$ in 1% intervals.

The measurements at high turbulence show little of the fluctuations in rotor wake thickness or accumulation of low energy fluid that were observed in the low turbulence measurements. This suggests that higher levels of turbulence have reduced the magnitude of wake–wake interactions and the overall periodic unsteadiness of flow.

The turbulence level is also observed to have a strong influence on mixing processes. In the test cases at high turbulence the location of IGV wakes are only indicated by a slight velocity defect and increase in turbulence. These observations suggest the higher turbulence level has accelerated the mixing out of the IGV wakes resulting in a more uniform turbulence and velocity flow field.

5.3.1 Turbulence Grid–IGV Blade Row Clocking Effects

The measurements presented in Section 5.3 were made with the turbulence grid wakes centred in the IGV passage ($g/S = 0.5$). It was also suggested in Section 5.2 that this configuration gave a more uniform turbulence distribution. Figure 5.5 compares the flow field resulting from two main grid–IGV clocking configurations. The case with the grid wakes incident on the IGV blade row is shown in the top plot ($g/S = 0.0$) and the case with the grid wakes in the IGV passage is shown in the lower part ($g/S = 0.5$). The case $g/S = 0.0$ shows greater levels wake–wake interaction, periodic events and also variation of turbulence and velocity. The total disturbance level between the IGV wake streets is significantly higher than in the cases without the grid. This is principally due to the unsteady disturbance component $\tilde{T}u$ associated with regions of low energy rotor wake fluid accumulation. The lower degree of wake uniformity for $g/S = 0.0$ is associated with the reduced wake dispersion effects produced by the lower random turbulence Tu in the mid IGV passage region where the grid turbulence is weaker.

5.3.2 Ensemble Averaged Velocity-Time Traces

A comparison of the ensemble averaged velocity traces at various pitchwise positions is shown in Fig 5.6 (medium compressor loading). The measurements at low turbulence are shown in the upper part and the measurements at high turbulence are shown in the lower part. A time shift has been applied to allow wake passing signatures at different pitchwise positions to be compared in the same relative time frame. The low turbulence results show a large variation in terms of both wake signature and velocity.

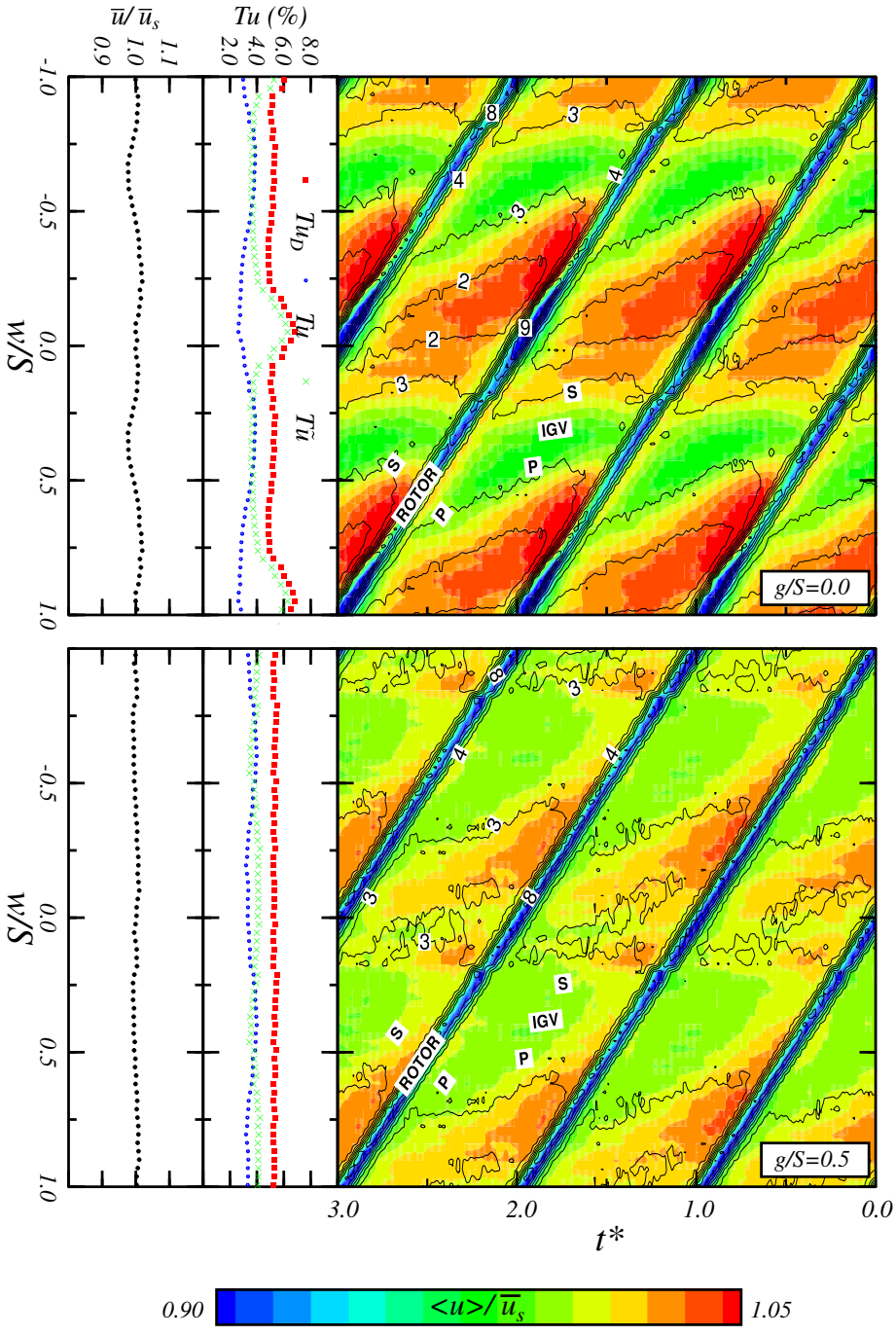

Figure 5.5: Unsteady flow field in the rotor–stator axial space at medium compressor load with the turbulence grid ($\phi = 0.675$ and $Re_c = 120000$). Top: grid wakes incident on IGV blade row ($g/S = 0.0$). Bottom: grid wakes in IGV passage ($g/S = 0.5$). Filled contours show ensemble-averaged velocity $\langle u \rangle / \overline{u}_s$. Line contours show ensemble-averaged turbulence level $\langle Tu \rangle >$ in 1% intervals.

The variation in wake signature is primarily due to local rotor wake fluid accumulation arising from wake–wake interaction effects. Some variation between traces would be caused by the velocity defect associated with the IGV wake street. The high turbulence measurements show significantly less variation with pitchwise position. These observations are consistent with ensemble averaged results presented in Section 5.3.

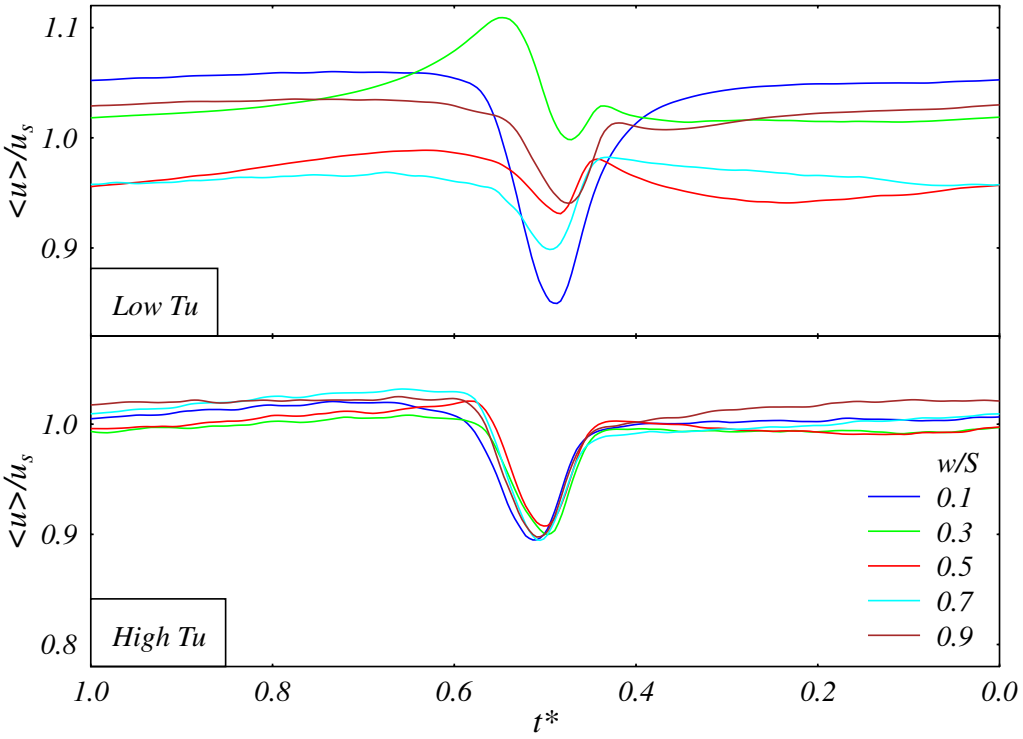

Figure 5.6: Temporal variation in velocity at several circumferential positions for medium load ($\phi = 0.675$ and $Re_c = 120000$). Common time origin $t^* = 0.5$ at centre of rotor wake disturbance.

5.4 Integral Length Scale

The integral length scale or *macro* scale of free-stream turbulence is generally acknowledged as an important factor influencing the process of boundary layer transition [111]. Despite this, there have been relatively few studies on the topic. Abu Ghannam and Shaw [1] studied natural transition on a flat plate for various inlet turbulence levels and observed little dependence on grid size. However, their study was concerned with the onset and length of transition rather than changes in the breakdown process.

The integral length scale is representative of the larger scales or eddy sizes present in a flow and may be expressed as

$$\Lambda = \overline{u} \int_0^\infty R_{ii}(t) d(t) \tag{5.1}$$

where the R_{ii} is the autocorrelation function of the velocity signal u_i.

Tritton [171] points out that the shape of the autocorrelation function can provide some qualitative information about the underlying structure of turbulence. The autocorrelation function in flows with a wide range of turbulence scales will generally take longer to reach zero correlation. Flows with coherent vortical structures, such as periodic eddy shedding, will have have dominant components within a narrow frequency range. Such components create oscillations in the autocorrelation function which can significantly decrease the time taken to reach zero correlation. The choice of the integration limit is an important consideration since there are very few situations where it is practical to evaluate an infinite dataset. O'Neill et al. [124] found significant differences between integral length scales evaluated using four different methods detailed in Tritton [171]. In this study, the integration limit was specified as the first zero of the autocorrelation function.

Camp and Shin [18] developed a method for evaluating the integral length scale of turbulence in turbomachinery flows from single element hot-wire measurements. In particular, the method addressed the problem of periodic flow events that are common in turbomachinery flows. The oscillations imposed by such events are not representative of true stochastic turbulence. Camp and Shin [18] applied a Fourier transform to convert velocity-time data to the amplitude-frequency domain. This allowed dominant frequency components, such as rotor passing events and associated harmonics, to be identified and removed. The signal was then reconstructed by inverse Fourier transform for analysis.

Hughes [83] extended this method to allow integral length scale to be determined from the shorter data records used in Section 5.3. Longer traces consisting of 4096 points were constructed by joining together 4 traces acquired on separate rotor revolutions. Hughes [83] studied the repeatability of this approximate method by comparing integral length scales obtained from longer singularly-acquired data traces. Only minor differences were reported and the method was considered suitable for estimating integral length scale.

In this study, an average integral length scale was obtained at each of the 32 pitchwise stations by averaging 10 independently determined values. These values were then used to determine pitchwise averages as presented in Table 5.1.

Loading	ϕ (V_a/U_{mb})	Λ/c Low Tu	Λ/c High Tu
High	0.600	6.0%	7.2%
Medium	0.675	4.8%	7.6%
Low	0.840	3.5%	11.4%

Table 5.1: Pitchwise averaged integral length scale for low and high turbulence cases (medium loading $\phi = 0.675$)

The results shown in Table 5.1 indicate an increase in integral length scale with turbulence level. On first inspection this may appear as a surprising trend; however, some explanation may be offered by considering the effect of wake dispersion on the integral length scale. By definition, integral length scale is a time-mean property of turbulence in the flow. The flow at a single pitchwise station periodically experiences turbulence from three main sources: rotor, IGV and turbulence grid. The integral length scale of turbulence generated from each of these sources is expected to increase with distance from the source [135]. For example, the integral length scale from the rotor wakes is expected to be approximately $2 - 3\%$c (see Camp and Shin [18]). The turbulence from the IGV and turbulence grid, having travelled a greater streamwise distance, is expected to have a significantly larger integral length scale. In the low turbulence case, the flow is likely to be dominated by a combination of turbulence from both IGV and rotor wake fluid: this is consistent with the values shown in Table 5.1. In Section 5.3, the turbulence generated by the the grid was found to accelerate the mixing of IGV wake streets, resulting in a greater pitchwise dispersion of IGV wake fluid. This effect, combined with turbulence from the grid, would be expected to raise

the value of integral length scale in the high turbulence case.

The results in Table 5.1 also show a variation of integral length scale with loading. As noted in Section 5.3, compressor loading influences the level of turning through the rotor blade row, and thus the amount of rotation of the IGV wake segments. Increasing compressor loading spreads the IGV wakes across a wider pitchwise distance and also increases the thickness of rotor wakes. These factors are expected to cause the integral length scale to vary with loading. Similar variations with compressor loading were also noted by Camp and Shin [18].

5.5 Conclusions

A turbulence generating grid was installed at the compressor inlet to raise the background level of turbulence in the research compressor. The pitchwise flow field was surveyed by a single-element hot-wire probe and compared with previous measurements by Hughes [83] made in the natural low turbulence configuration of the compressor. The increased turbulence level was shown to significantly influence the wake dispersion and IGV wake – rotor wake interaction processes. The IGV wake fluid was more widely diffused by the grid turbulence resulting in reduced values of IGV wake velocity defect. The periodic unsteadiness of the flow field was greatly reduced because of less accumulation of low energy rotor wake fluid on the suction surface of the IGV wake street. The implications of the measured flow fields on the unsteady stator boundary layer behaviour is discussed in Chapter 6. It is concluded that reliable predictions of downstream blade row behaviour require accurate modelling of the effects of free-stream turbulence on the dispersion and interaction of wakes from blade rows further upstream.